

Theoretical Study of the  $\text{H}_2 + \text{NO}$  and Related Reactions of  $[\text{H}_2\text{NO}]$  IsomersRaman Sumathi,<sup>†</sup> Debasis Sengupta, and Minh Tho Nguyen\*

Department of Chemistry, University of Leuven, Celestijnenlaan 200F, B-3001 Leuven, Belgium

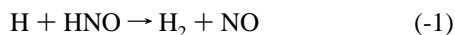
Received: December 11, 1997; In Final Form: February 20, 1998

Mechanisms of the reactions occurring on the multichannel lowest doublet potential energy surface of the  $[\text{H}_2\text{NO}]$  system containing  $\text{H}_2\text{NO}$ ,  $\text{HNOH}$ , and  $\text{NOH}_2$  intermediates and including the  $\text{H}_2 + \text{NO}$ ,  $\text{NH}_2 + \text{O}$ ,  $\text{NH} + \text{OH}$ , and  $\text{H} + \text{HNO}$  entry channels have been probed using unrestricted coupled-cluster formalism. Also, the transition structure on the doublet energy surface for the direct hydrogen abstraction from  $\text{H}_2 + \text{NO}$  yielding  $\text{H} + \text{HNO}$  has been identified. The energetic and molecular parameters derived from coupled cluster singles and doubles with triples correction (CCSD(T)) calculations using the 6-311++G(3df,3pd) basis set, based on their respective optimized geometries obtained with a 6-311++G(d,p) basis set, have then been utilized to compute the apparent rate constants of the different competitive channels in the  $[\text{H}_2\text{NO}]$  system within the framework of a quantum version of Rice–Ramsperger–Kassel theory (QRRK). The  $\text{H}_2 + \text{NO}$  reaction is found to be a rather slow reaction, and it occurs via bimolecular hydrogen abstraction. The calculated total rate constant for this reaction at 2000 K and 1 atm is  $2.35 \times 10^8 \text{ cm}^3 \text{ mol}^{-1} \text{ s}^{-1}$ . Stabilization of  $\text{NH}_2\text{O}$  or  $\text{HNOH}$  intermediates plays a minor role in the kinetics of  $\text{NH}_2 + \text{O}$  reaction which is dominated by the dissociation products,  $\text{HNO} + \text{H}$ ,  $\text{NH} + \text{OH}$  and  $\text{H}_2 + \text{NO}$ . The  $\text{H} + \text{HNO}$  reaction kinetics has only 10% contribution from addition/isomerization/dissociation paths at 2000 K and 1 atm.  $\text{H}_2 + \text{NO}$  and  $\text{H} + \text{HNO}$  are expected to be the competitive products in the reaction of  $\text{OH}$  with nitrene. The calculated standard heats of formation are  $\Delta H_f^{298}(\text{NH}_2\text{O}) = 17.5 \pm 2$  and  $\Delta H_f^{298}(\text{HNOH}) = 23.7 \pm 2 \text{ kcal/mol}$ .

## Introduction

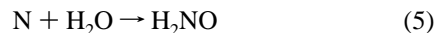
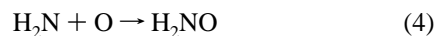
The  $[\text{H}_2\text{NO}]$  isomeric system is of wide interest. The  $\text{H}_2\text{NO}$  isomer represents the simplest member of the family of nitroxide radicals whose particular electronic properties and high thermodynamic stabilities have classically been employed in spin-labeling experiments in electron spin resonance (ESR) and other related spectrometries.<sup>1</sup> They are used as magnetic probes in physical, chemical, and biological experiments.<sup>1</sup> Also,  $(\text{H}_2\text{NO})$  species are expected to be involved in the  $\text{H}_2 + \text{NO}$  and  $\text{H} + \text{HNO}$  reactions, which play an important role in the rate mechanism of processes such as the inhibition of combustion by nitric oxide, the reaction of radicals and  $\text{NO}$  in the atmosphere, the catalyzed recombination of  $\text{H}$  and  $\text{OH}$  radicals in flames and the combustion of nitrogen-containing fuels. Information on the rate of these reactions have been used in the modeling of energy release in advanced propellants as well as to predict the pollutant formation and destruction in the combustion of nitrogen fuels.<sup>2</sup>

The  $\text{NO}/\text{H}_2$  reaction system has been experimentally investigated by several groups<sup>3–6</sup> at different temperature ranges (2000–4500 K) and initial concentration ratios and by using a variety of detection techniques to monitor the  $\text{NO}$  disappearance. A large consensus appears to emerge from these studies indicating that the initial phase is actually an hydrogen abstraction (eq 1).



Ab initio molecular orbital calculations<sup>7,8</sup> have indicated that reaction 1 is highly endothermic and proceeds nearly without

an activation barrier except for the reaction endoergicity. Ando and Asaba<sup>3</sup> reported the first shock-tube measurement of its rate coefficient,  $k_1 = 3.16 \times 10^{13} \exp(-27780 \text{ K}/T) \text{ cm}^3 \text{ mol}^{-1} \text{ s}^{-1}$  over the temperature range 2300–3500 K. Natarajan et al.<sup>5</sup> reported a value of  $k_1 = 1.5 \times 10^{13} \exp(-26165 \text{ K}/T) \text{ cm}^3 \text{ mol}^{-1} \text{ s}^{-1}$  by using atomic resonance absorption spectroscopy. Simultaneously, the high-temperature rate measurements of the reverse process, the  $\text{H} + \text{HNO}$  reaction (eq -1), have also been performed by a number of authors<sup>9–25</sup> but the disagreement on its rate constant still persists.<sup>7</sup> On the basis of variational transition-state theory and large-scale multireference configuration interaction calculations, Page et al.<sup>7</sup> predicted a rate constant of  $k(T) = 7.406 \times 10^{-13} T^{0.720} \exp(-329.1 \text{ K}/T) \text{ cm}^3 \text{ mol}^{-1} \text{ s}^{-1}$  for  $\text{H} + \text{HNO}$ , which is an order of magnitude larger than its recommended value.<sup>15</sup> The hydrogen addition reactions to  $\text{HNO}$  (eq 2) and (eq 3) have also been investigated in a recent theoretical study<sup>16</sup> which showed that they are much slower than the hydrogen abstraction (equation -1). However, it is worthwhile to mention that these variational transition state theory calculations were only performed on the isolated steps, viz.,  $\text{H} + \text{HNO} \rightarrow \text{NH}_2\text{O}$  and  $\text{H} + \text{HNO} \rightarrow \text{HNOH}$  of the complex multichannel  $\text{H} + \text{HNO}$  reaction.



<sup>†</sup> On leave from Manonmanium Sundaranar University, Tirunelveli-627 002, India.

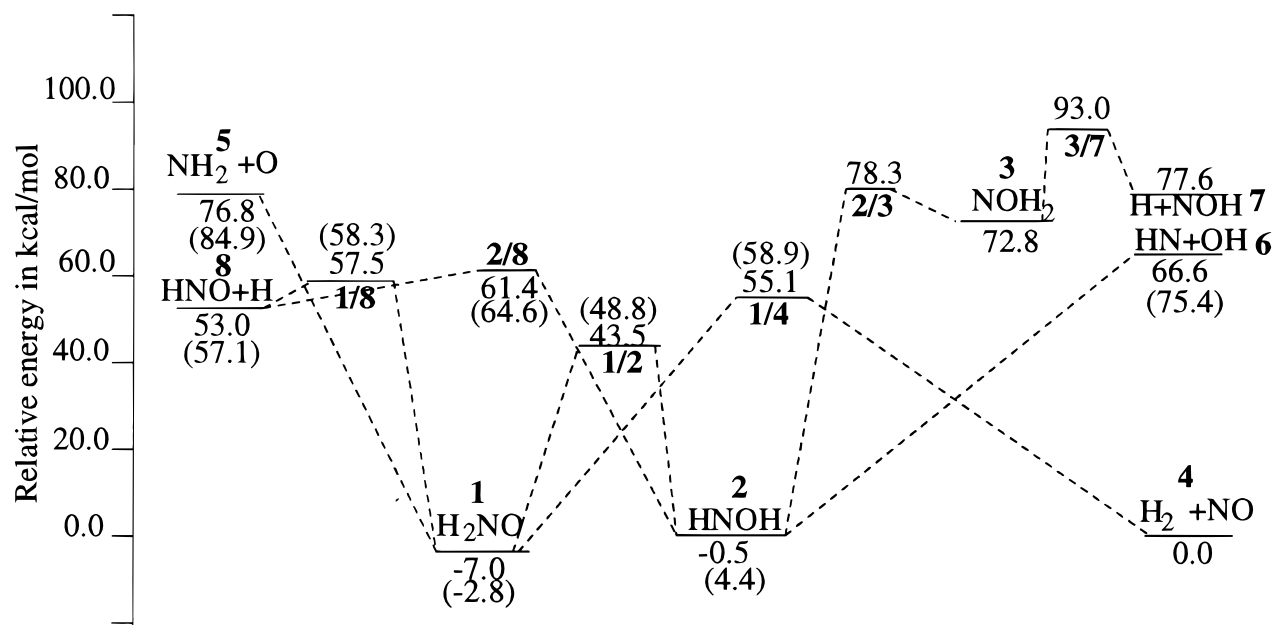


**Figure 1.** Overall profile of the potential energy surface for the [H<sub>2</sub>NO] system calculated at CCSD(T)/6-311++G(3df,3pd)//CCSD(T)/6-311++G(d,p)+ZPE level of theory. Values in parentheses correspond to the G2 level of theory taken from ref 36.

The NH<sub>2</sub>O radical is, however, likely to be a primary adduct of reactions 4 and 5 and once formed can undergo fragmentations (−2) and (7) or form (6) via HNOH. While the reaction of the amidogen radical<sup>4</sup> with atomic oxygen has been investigated extensively both experimentally<sup>17–19</sup> and theoretically,<sup>8,20,21</sup> the reaction of water and atomic nitrogen has not been studied yet. Calculations on the lowest quartet potential energy surface,<sup>20,21</sup> suggested that the hydrogen abstraction channel (NH<sub>2</sub> + O → NH + OH) are less favored than the direct recombination giving the primary H<sub>2</sub>NO adduct, and the reason for the observation of an abnormal OD product rotational distribution<sup>21</sup> remains unclear. Although the H<sub>2</sub>NO potential energy surface has been the subject of a large number of ab initio molecular orbital studies,<sup>7,8,20–26</sup> most of them have, on one hand, mainly focused on small portions of the surface, and on the other hand, the existing kinetic analyses<sup>7,16,21</sup> based on canonical variational transition-state theory using molecular orbital (MO) results as inputs have considered only the individual elementary steps. It is, however, well established that in the study of reactions involving multiple and competing channels, characterized by formation of energized complexes, the apparent rate constant of a certain reaction cannot be treated by considering them as separate elementary single-step reactions; all the possible channels need to be included in order to model the corresponding apparent rate constants. The purpose of the present study is 2-fold; in the first part we have reexplored as complete as possible the low-lying doublet [H<sub>2</sub>NO] energy surface using reliable and, more importantly, uniform ab initio MO calculations. The geometrical and thermochemical results thus obtained have subsequently been utilized in the second part to calculate the rate constants of various reactions occurring on the same [H<sub>2</sub>NO] potential energy surface but differing from each other by the entry channels. For this latter purpose we have made use of a rather simple quantum statistical treatment<sup>27,28</sup> whose basic equations and performance have been discussed in detail in our recent papers.<sup>29–34</sup>

### Molecular Orbital Calculations

Ab initio molecular orbital calculations were carried out using the Gaussian 94 set of programs.<sup>35</sup> The open shell calculations

were performed using the unrestricted Hartree–Fock formalism. The low-lying doublet potential energy surface was initially mapped out using second-order perturbation theory calculations (UMP2) in conjunction with the 6-31G(d,p) basis set. Stationary points were characterized by harmonic vibrational frequency analyses at this level. After establishing the different minimum energy paths by using intrinsic reaction coordinate (IRC) calculations, geometrical parameters of the relevant equilibrium and transition structures were then reoptimized by a coupled-cluster electron correlation method that includes all the single and double excitations plus a perturbational estimate for the connected triple excitations, CCSD(T), with the larger 6-311++G(d,p) basis set. Finally electronic energies of stationary points were computed using the coupled-cluster method and optimized geometries with the more extended 6-311++G(3df,3pd) basis set in order to obtain improved estimates for their relative energies. In the coupled-cluster calculations, only the valence electrons are included in the correlation procedure. The zero-point energies were derived from harmonic vibrational wavenumbers at the UMP2/6-31G(d,p) level and scaled down by a uniform factor of 0.94. Throughout this paper, bond lengths are given in angstroms, bond angles in degrees, and zero-point and relative energies in kcal/mol, unless otherwise stated.

### Results and Discussion

Let us first describe briefly the essential features of the potential energy surface (PES) related to [H<sub>2</sub>NO] schematically shown in Figure 1. Each stationary point in Figure 1 is labeled with a number in order to facilitate an easy discussion. While the equilibrium positions are associated with the numbers from 1 to 8, the transition structures are defined by X/Y where X and Y are the two connected equilibrium structures. As can be seen, the PES consists of three isomers, namely, NH<sub>2</sub>O **1**, HNOH **2**, and NOH<sub>2</sub> **3**, and the different first-order saddle points connecting these minima to different product limits, viz., H<sub>2</sub> + NO **4**, NH<sub>2</sub> + O **5**, HN + OH **6**, NOH + H **7**, and H + HNO **8**. The CCSD(T)/6-311++G(d,p) optimized geometries of the transition states 1/2, 2/3, 1/4, 1/8, 2/8, 3/7, and the direct hydrogen abstraction transition state 4/8 are also shown in

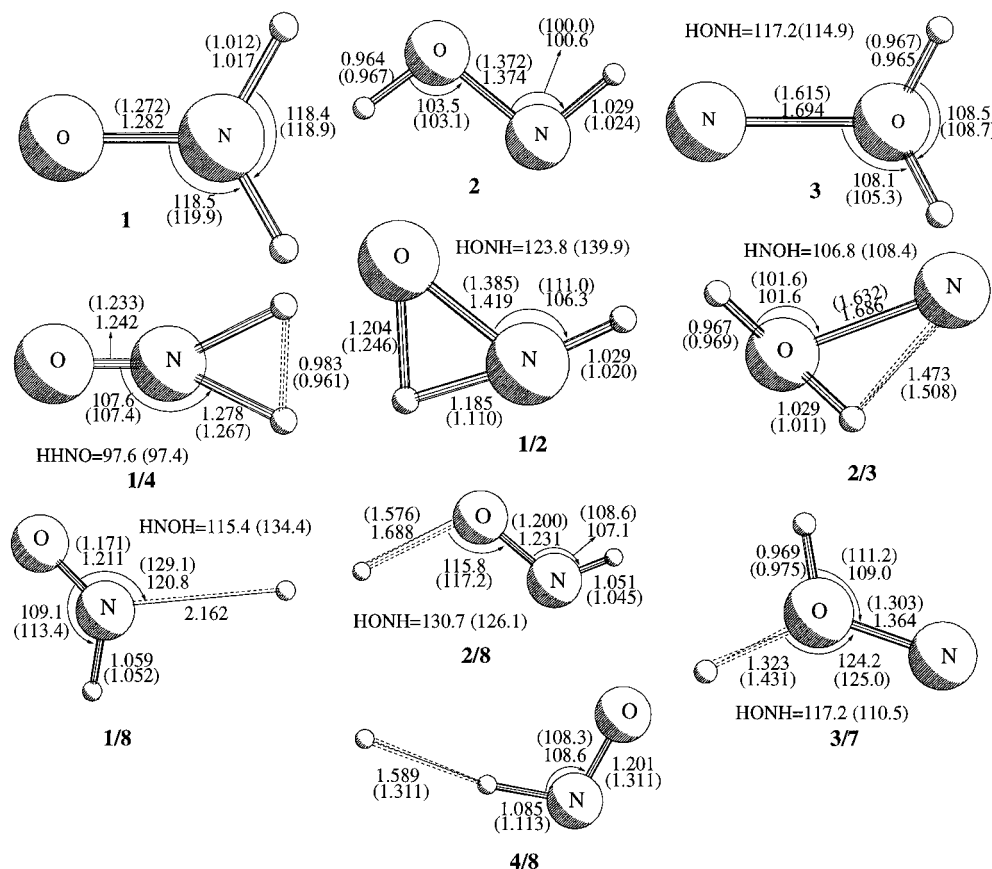


**Figure 2.** CCSD(T)/6-311++G(d,p) optimized geometries (in Å and deg) of the stationary points **1**, **2**, **3**, **1/2**, **2/3**, **1/4**, **1/8**, **2/8**, **3/7**, **4/8** in the [H<sub>2</sub>NO] system. Values in parentheses correspond to the UMP2/6-31G(d,p) level of theory.

**TABLE 1: Calculated CCSD(T)/6-311++G(3df,3pd) Total Energies in atomic units and ZPE in kcal/mol for Species Involved in the [H<sub>2</sub>NO] PES**

species	total energy <sup>a</sup>	ZPE <sup>b</sup>
H <sub>2</sub> NO <b>1</b>	-130.908 566	17.2
HNOH <b>2</b>	-130.898 551	17.4
NOH <sub>2</sub> <b>3</b>	-130.780 009	16.3
<b>1/2</b>	-130.822 832	13.8
<b>2/3</b>	-130.770 758	15.8
<b>1/4</b>	-130.799 874	10.7
<b>1/8</b>	-130.770 758	15.8
<b>2/8</b>	-130.789 900	10.8
<b>3/7</b>	-130.741 076	11.8
<b>4/8</b>	-130.800 055	8.3

<sup>a</sup> Based on optimized geometries at the CCSD(T)/6-311++G(d,p) level. <sup>b</sup> Zero-point energies using unscaled frequencies at the UMP2/6-31G(d,p) level.

Figure 2. The numbers in parentheses refer to the results obtained at the UMP2/6-31G(d,p) level of calculation. The CCSD(T)/6-311++G(3df,3pd)/CCSD(T)/6-311++G(d,p) energies are summarized in Table 1 and shown in Figure 1 relative to that of the H<sub>2</sub> + NO limit **4** with appropriate zero-point vibrational energy corrections using UMP2 frequencies. The values given in parentheses represent the G2 values obtained by Wolf et al.<sup>36</sup> The unscaled harmonic vibrational frequencies of the isomers and of the various saddle points are listed in Table 2, as they are of interest to the modeling kineticists. Energetically, H<sub>2</sub>NO **1** was found to be more stable than *trans*-HNOH **2** by 7 kcal/mol. Three possible unimolecular dissociation pathways for NH<sub>2</sub>O have been identified, namely dissociation into NH<sub>2</sub> + O without a distinct transition state, concerted elimination of H<sub>2</sub> and NO through a three-membered transition structure, **1/4** and the dissociation into H + HNO via

**1/8**. The molecular elimination of H<sub>2</sub> involves a barrier of 62.1 kcal/mol and the barrier height for the H + HNO product formation is found to be 64.5 kcal/mol. The reverse barrier for the combination of H + HNO → HONO was calculated to be 8.4 kcal/mol, and this value is in close agreement with G2 results (7.57 kcal/mol) of Wolf et al. but differs somewhat from the value of 3.5 kcal/mol reported by Lin et al.<sup>37</sup> for the same process using G2M calculations. In that report, the authors have also not identified **1/8** and considered the H + HNO → H<sub>2</sub>NO as a barrierless process. In contrast, in the present investigation, the corresponding process was found to have a barrier as large as 4.5 kcal/mol. In addition to these dissociations, NH<sub>2</sub>O can undergo isomerization to *trans*-HNOH.

*trans*-HNOH **2** can undergo either O-H bond cleavage giving rise to HNO + H radicals or N-O bond cleavage to HN + OH. The former process was found to proceed via the specific transition state, **2/8**, and to involve a barrier height of 61.9 kcal/mol. The latter process is a direct dissociation and the barrier height thus equals the reaction endoergicity. The 1,2-hydrogen migration in *trans*-HNOH is associated with a high barrier (78.8 kcal/mol) and the resulting isomer NOH<sub>2</sub> **3** is characterized by a shallow potential well (5.5 kcal/mol).

The calculated reaction energies at the CCSD(T)/6-311++G-(3df,3pd) level have been used in conjunction with the known heats of formation of H and HNO to obtain  $\Delta H_f^0$  for the addition species. For example,  $\Delta H_f^0(\text{H}_2\text{NO}) = \Delta H_f^0(\text{H}) + \Delta H_f^0(\text{HNO}) + \Delta H_R^0$  where  $\Delta H_R^0$  is the zero-degree enthalpy of reaction. By this procedure we obtain  $\Delta H_{f,0}^0(\text{H}_2\text{NO}) = 18.3$ ,  $\Delta H_f^0(\text{HNOH}) = 24.8$  kcal/mol. We also obtain the standard heats of formation,  $\Delta H_f^{298}(\text{NH}_2\text{O}) = 17.5$  and  $\Delta H_f^{298}(\text{HNOH}) = 23.7$  kcal/mol for both the species with a probable error of  $\pm 2$  kcal/

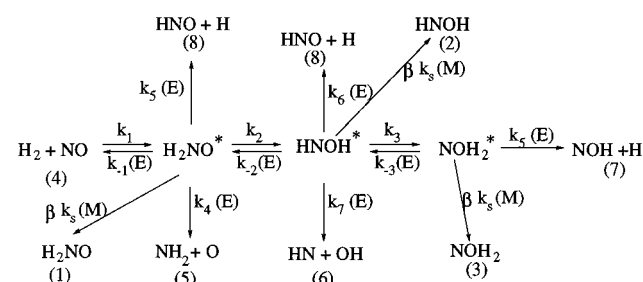
**TABLE 2: Unscaled UMP2/6-31G(d,p) Harmonic Vibrational Frequencies of the Minima and Saddle Points in H<sub>2</sub>NO PES**

H <sub>2</sub> NO	HONO	NOH <sub>2</sub>	1/4	1/2	2/3	1/8	2/8	3/7	4/8
248.8	787.3	522.4	<b>2137.5i</b>	<b>1850.8i</b>	<b>1171.4i</b>	<b>974.4i</b>	<b>2021.3i</b>	<b>1218.1i</b>	<b>1458.3i</b>
1292.8	1156.9	730.1	1006.7	192.1	891.2	456.3	606.8	837.4	188.1
1524.5	1287.7	788.1	1171.1	1300.7	1396.7	629.1	672.9	1044.5	772.3
1723.7	1603.8	1623.2	1195.9	1503.8	1699.7	1458.3	1506.5	1300.5	1440.3
3542.2	3502.6	3796.3	1593.2	3091.2	3232.7	2825.3	1578.2	1375.9	1583.6
3700.1	3853.5	3938.0	2494.6	3536.9	3845.0	3047.3	3171.7	3702.3	1828.6

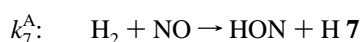
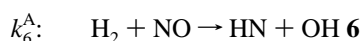
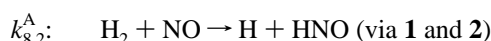
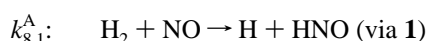
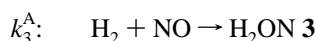
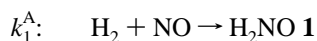
mol. These values are in close agreement with those predicted by Soto et al.<sup>21</sup>

We now turn to the second part of this work which is the kinetic analysis of the various channels associated with the [H<sub>2</sub>-NO] system. Thus, the apparent rate constants of the reactions (A) H<sub>2</sub> + NO, (B) NH<sub>2</sub> + O, (C) NH + OH, and (D) H + HNO have been computed using QRRK theory. Various product channels of these reactions are summarized in Scheme 1. We use the potential energy surface obtained at the CCSD-(T)/6-311++G(3df,3pd)/CCSD(T)/6-311++G(d,p) level and the vibrational frequencies and rotational constants calculated at the UMP2/6-31G(d,p) level as input parameters for the QRRK calculations. Recent publications<sup>24–34,38</sup> reveal that processes involving high energy chemically activated adducts with non-Boltzmann distribution can be characterized by the simple QRRK method with reasonable accuracy. In essence, quantum Kassel theory employs statistical mechanics to calculate the probability that sufficient energy will be localized in a given oscillator for reaction to occur. Weston et al.<sup>39</sup> have outlined the advantages and limitation of this approach over the more rigorous RRKM treatment. In the literature, most of the RRKM studies calculated the *A* factor for dissociation from the assumed properties of the transition state and the reactant, i.e., the vibrational and internal rotor frequencies, the state densities, and rotational parameters. As a consequence, the uncertainties in the input parameters may restrict its predictive values, unless significant effort is put into the assignment. However, in QRRK one could either use the experimentally measured value for the *A* factor or estimate the same based on isoelectronic or structurally similar reactants with known kinetic parameters. Though QRRK is less rigorous compared to its complementary well-established technique, RRKM, it provides a simpler way to treat the kinetics of the multichannel system with many dissociation pathways. Since our interest is to obtain the rate coefficient of various reactions on the [H<sub>2</sub>,N,O] potential energy surface and at the same level, we employ here the less rigorous QRRK technique. It is appropriate to mention that tunneling corrections have not been included in this work even though the potential surface involves primarily the migration of the hydrogen atoms. The neglect of tunneling corrections is justifiable due to the fact that the lowest temperature employed in the present study is 300 K. Furthermore, the reactants, NH<sub>2</sub> + O (reaction B) and NH + OH (reaction C) are disposed energetically above the isomerization/hydrogen migration transition structures, viz., 1/2, 1/4, 1/8, 2/8, and hence we expect the tunneling mechanism to be unimportant in their reaction kinetics. On the contrary, tunneling may play a role in the kinetics of H + HNO (reaction D) system, especially at the entrance channel (H + HNO → H<sub>2</sub>NO and + HNO → HNOH). However, as will be shown shortly, the kinetics of this reaction is dominated by the direct hydrogen abstraction channel and the barrier for this process is negligibly small (0.16 kcal/mol). It is therefore clear that the tunneling phenomenon is of less importance in the kinetics of these reactions at temperatures above 300 K.

**QRRK Analysis of the H<sub>2</sub> + NO Reaction (Reaction A).** The apparent rate constants of various channels for the H<sub>2</sub> +

**SCHEME 1**

NO reaction are defined as



The apparent rate constant for stabilization of, say **1**, was calculated by the rate expression:

$$k_1^A = \beta k_s[M] \sum_{E_{\text{crit}}} [1^*] f(E) / [\text{H}_2][\text{NO}]$$

Similarly, the apparent rate constant for a dissociation pathway, for example,  $k_{8,1}^A$ , was obtained from

$$k_{8,1}^A = \sum_{E_{\text{crit}}} k_5(E) [1^*] f(E) / [\text{H}_2][\text{NO}]$$

where [1\*] is the steady-state concentration of **1** (see Scheme 1). Similar expressions were followed to calculate other apparent rate constants for other reactions. The expression for  $f(E)$ , the chemical activation distribution function, was taken from ref 40. *M* is the bath gas (N<sub>2</sub> for the present study) and  $k_i(E)$  are the energy-dependent unimolecular rate constants, which are calculated using QRRK theory. The steady-state concentration of the isomers can readily be expressed in terms of  $k_i(E)$ . The method of calculation of energy dependent unimolecular rate constant has been discussed in detail elsewhere.<sup>27,28</sup>

The frequency factors for isomerization of chemically activated species and for the unimolecular reactions with specific transition states were calculated as

$$A_i = \frac{k_B T}{h} \frac{Q^\ddagger}{Q_i}$$

where  $k_B$  is the Boltzmann constant,  $h$  the Planck's constant,  $T$  the temperature in kelvin, and  $Q_i^\ddagger$  and  $Q_i$  are the complete partition functions for the respective transition state and the reactant, respectively. The partition functions were obtained from our ab initio calculated harmonic vibrational frequencies and moments of inertia at the UMP2/6-31G(d,p) level. The frequency factors for the barrierless recombination and dissociation reactions, viz.,  $\text{NH}_2 + \text{O} \rightarrow \text{NH}_2\text{O}$ ,  $\text{NH}_2\text{O} \rightarrow \text{NH}_2 + \text{O}$ ,  $\text{NH} + \text{OH} \rightarrow \text{HNOH}$  and  $\text{HNOH} \rightarrow \text{NH} + \text{OH}$  were taken from Dean et al.,<sup>28</sup> and the values used are, respectively,  $7 \times 10^{13} \text{ cm}^3 \text{ mol}^{-1} \text{ s}^{-1}$ ,  $1.32 \times 10^{15} \text{ s}^{-1}$ ,  $4.0 \times 10^{13} \text{ cm}^3 \text{ mol}^{-1} \text{ s}^{-1}$ , and  $7.18 \times 10^{14} \text{ s}^{-1}$ . The concerted addition rate constant,  $k_1$ , for the combination of  $\text{H}_2$  and  $\text{NO}$  giving **1** was calculated by using the Arrhenius rate expression with 55.1 kcal/mol activation barrier.

For the description of the collisional stabilization, we adopted the weak collision model suggested by Troe,<sup>41,42</sup> and the collision rate is considered to be a product of the Lennard-Jones collision frequency,  $Z_{\text{LJ}}$ , and collision efficiency,  $\beta$ . The collision efficiency,  $\beta$ , was calculated from<sup>42</sup>

$$\beta/(1 - \beta^{1/2}) = -\langle \Delta E \rangle / F_E k_B T$$

The value of  $F_E$  was assumed to be 1.15, and  $-\langle \Delta E \rangle$ , the average energy transferred per collision, was taken as 0.382 kcal/mol for  $\text{N}_2$  as bath gas following the reference of Hippler et al.<sup>43</sup>

The PES reported earlier by Melius and Binkley<sup>44</sup> and Walch<sup>8</sup> have apparently missed the important link between  $\text{NH}_2\text{O}$  and  $\text{H}_2 + \text{NO}$  stationary points, which was later established by Wolf et al.<sup>36</sup> As can be seen from Figure 1, the direct hydrogen abstraction involves a lower barrier (53.0 kcal/mol) and hence is expected to compete with the  $\text{NH}_2\text{O}$  adduct formation pathway. Moreover, the transition structure **4/8** corresponding to a direct hydrogen abstraction process is looser and is characterized by low-frequency vibrations as compared to **1/4**. As a result, the frequency factor for bimolecular abstraction is high and is of the order of  $3.0 \times 10^{13} \text{ cm}^3 \text{ mol}^{-1} \text{ s}^{-1}$  at 300 K. Consequently, at all temperatures, the rate constant for bimolecular abstraction is around 4 orders of magnitude higher than the total addition rate constant of reaction A, which was calculated as the sum of all corresponding apparent rate constants. Figure 3 shows the variation of the total bimolecular abstraction ( $k_{\text{BA}}^{\text{A}}$ ) and addition ( $k_{\text{T}}^{\text{A}}$ ) rate constants as a function of temperature. The total rate constant,  $k_{\text{T}}^{\text{A}}$  is thus mainly contributed by the  $k_{8,1}^{\text{A}}$ . The variation of other individual apparent rate constants with temperature are not shown due to the unimportance of the adduct formation in the  $\text{H}_2 + \text{NO}$  reaction. Furthermore, the rate of the reaction is expected to be pressure independent as it proceeds completely via the direct bimolecular abstraction. Owing to its large barrier height, the reaction can have a measurable rate coefficient only at temperatures beyond 1000 K. The calculated rate constant at 2000 K is  $2.35 \times 10^8 \text{ cm}^3 \text{ mol}^{-1} \text{ s}^{-1}$  and is approximately an order of magnitude higher than the value obtained in the shock tube measurements by Ando and Asaba.<sup>3</sup> This mismatch could probably be due to the low-frequency vibration of the loose transition structure, **4/8**. The best least-squares fit to the values of  $k^{\text{A}}$  obtained from our calculations leads to an expression of

$$k^{\text{A}}(T) = 2.93 \times 10^6 T^{2.25} \exp(-25500/T)$$

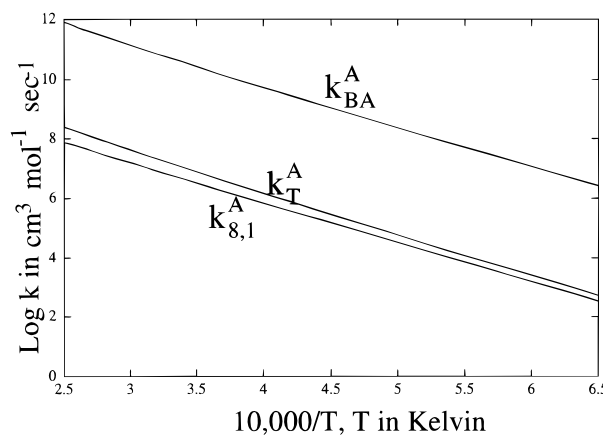


**Figure 3.** Plots of total association ( $k_{\text{T}}^{\text{A}}$ ) and direct hydrogen abstraction ( $k_{\text{BA}}^{\text{A}}$ ) rate constants of  $\text{H}_2 + \text{NO}$  system versus  $10^4/T$  (K) at 1 atm.

### QRRK Analysis of the $\text{NH}_2 + \text{O}$ Reaction (Reaction B).

As mentioned in the Introduction, three experimental reports are now available on the kinetics of the reaction of  $\text{NH}_2$  with atomic oxygen. Gehring et al.<sup>45</sup> reported a value of  $2.1 \times 10^{12} \text{ cm}^3 \text{ mol}^{-1} \text{ s}^{-1}$  using the absorption spectroscopic technique. Dransfeld et al.<sup>46</sup> subsequently derived a larger overall rate constant of  $(5.3 \pm 1.5) \times 10^{13} \text{ cm}^3 \text{ mol}^{-1} \text{ s}^{-1}$ , and they have estimated the branching ratio of 7:1 for product channels  $\text{HNO} + \text{H}$  and  $\text{NH} + \text{OH}$ . Recently, Adamson et al.<sup>17</sup> determined the overall rate constant to be  $(3.9 \pm 0.8) \times 10^{13} \text{ cm}^3 \text{ mol}^{-1} \text{ s}^{-1}$ . Dean et al.<sup>28</sup> have performed the QRRK kinetic analysis on this reaction using the PES provided by Melius and Binkley<sup>43</sup> using BAC-MP4 calculations. It should be noted that our present PES differs significantly from that of Melius and Binkley with respect to barrier heights. CASSCF calculations were also performed by Page et al.<sup>21</sup> on the quartet surfaces ( $^4\text{A}'$  and  $^4\text{A}''$ ) for the direct hydrogen abstraction, and these authors concluded that, below 2000 K, the  $\text{O} + \text{NH}_2$  reaction is dominated by the addition/isomerization/dissociation pathway. In view of its importance, we wish to reexamine the kinetics of this reaction using QRRK theory and the meaningful CCSD(T) PES.

The apparent rate constants of reaction B are defined as follows:

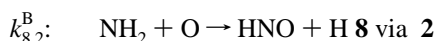
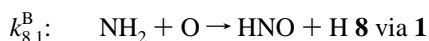
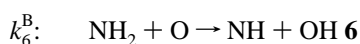
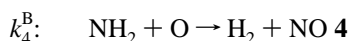
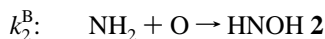
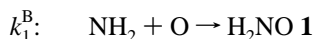
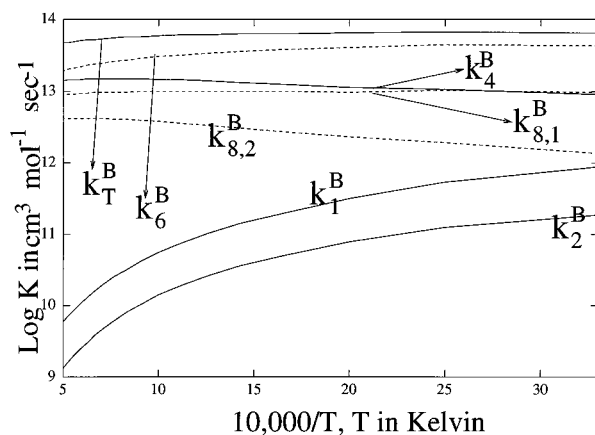
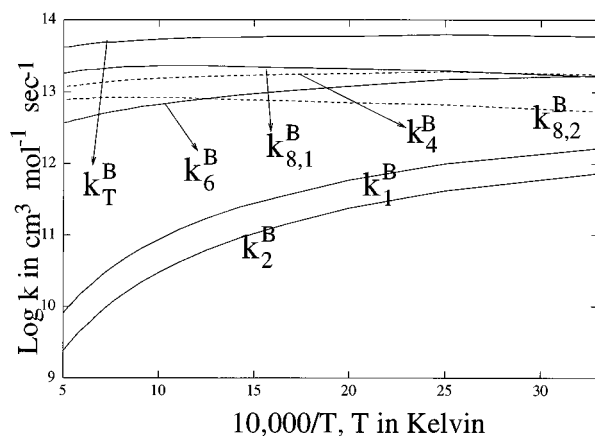


Figure 4 shows the variations of the apparent rate constants with temperature. The transition states for isomerization and both the dissociation paths from  $\text{NH}_2\text{O}$  are 33.3, 21.7, and 19.3 kcal/mol, respectively, below the initial energy of the adduct. Hence, the stabilization of  $\text{NH}_2\text{O}^*$  contributes only around 1% to the total rate constant at room temperature and 1 atm. Furthermore, the calculated barrier height for  $\text{H}_2 + \text{NO } \mathbf{4}$  formation from **1** is 2.4 kcal/mol lower than that for  $\text{HNO} + \text{H } \mathbf{8}$ . As a result, we observe an equally effective contribution of



**Figure 4.** Plots of log apparent rate constants and total rate constant of  $\text{NH}_2 + \text{O}$  reaction versus  $10^4/T$  (K) at 1 atm with  $A(6) = 7.18 \times 10^{14} \text{ s}^{-1}$ .



**Figure 5.** Plots of log apparent rate constants and total rate constant of  $\text{NH}_2 + \text{O}$  reaction versus  $10^4/T$  (K) at 1 atm with  $A(6) = 7.18 \times 10^{13} \text{ s}^{-1}$ .

$k_4^B$  and  $k_{8,1}^B$  to the total rate constant in contrast to the analysis of Dean et al.'s<sup>28</sup> using also the same kinetic treatment. The anomaly is no doubt due to the large barrier (79.0 kcal/mol) estimated by these authors for the  $\text{H}_2 + \text{NO}$  formation. Since the transition structure **1/8** is disposed energetically lower than **2/8**, the rate of  $\text{HNO} + \text{H}$  formation from **1** ( $k_{8,1}^B$ ) is higher than that from **2**. The value of the total rate constant calculated at 300 K and 1 atm is  $6.43 \times 10^{13} \text{ cm}^3 \text{ mol}^{-1} \text{ s}^{-1}$  and is in very good agreement with the experimental value of Adamson et al.<sup>17</sup> However, the predominant product channel in the kinetic analysis is the dissociation into the  $\text{NH} + \text{OH}$  rather than the experimentally observed  $\text{HNO} + \text{H}$  product. This is mainly due to the large magnitude of the frequency factor ( $A(6) = 7.18 \times 10^{14} \text{ s}^{-1}$ ) which we have adopted for the  $\text{NHOH} \rightarrow \text{NH} + \text{OH}$  channel. This frequency factor is around 2 orders of magnitude higher than derived from ab initio calculated frequencies and moments of inertia for the competitive channels  $\text{NH}_2\text{O} \rightarrow \text{HNO} + \text{H}$ ,  $\text{NH}_2\text{O} \rightarrow \text{H}_2 + \text{NO}$  and  $\text{HNOH} \rightarrow \text{HNO} + \text{H}$ . This indicates that  $A(6)$  has been overestimated. Nevertheless, there is no experimental report of rate constant for this reaction at high pressures. For the sake of comparison, we have carried out calculations by lowering the magnitude of  $A(6)$  by an order of magnitude, and the results are shown in Figure 5. We found then that the contribution of  $\text{NH} + \text{OH}$  product formation to the total rate constant decreases drastically, the predominant channel being the  $\text{H} + \text{HNO}$  formation, in line with the experimental observation. Hence, we conclude that the mismatch between the calculated and experimental branching

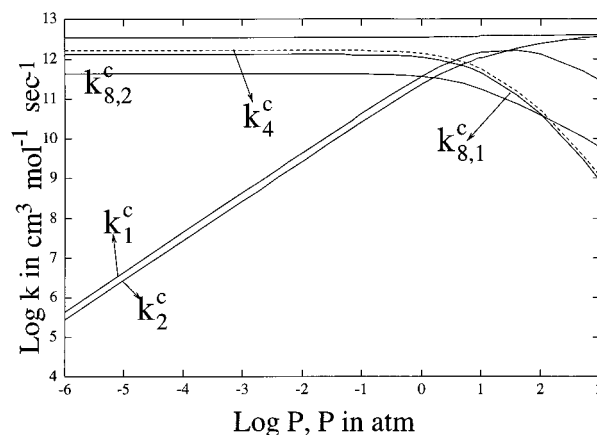


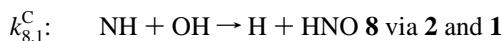
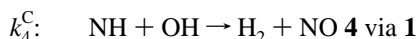
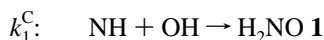
**Figure 6.** Plots of log apparent rate constants and total rate constant of  $\text{NH} + \text{OH}$  reaction versus log pressure.

ratio is due to the uncertainty in the magnitude of  $A(6)$ . We use, unless otherwise stated, as a reasonable estimate  $A(6) = 7.18 \times 10^{13} \text{ s}^{-1}$  in the rest of our investigations. The value of the total rate constant thus calculated at 300 K and 1 atm is  $5.89 \times 10^{13} \text{ cm}^3 \text{ mol}^{-1} \text{ s}^{-1}$ . Results of our calculation thus show that the total rate constant is nearly insensitive to the magnitude of this frequency factor. The three-parameter fit to the total rate constant leads to the expression

$$k^B(T) = 2.01 \times 10^{15} T^{-0.49} \exp(-213/T)$$

#### QRRK Analysis of the $\text{NH} + \text{OH}$ Reaction (Reaction C).

Cohen and Westberg<sup>47</sup> have reviewed this reaction and estimated the rate constants by analogy to the  $\text{OH} + \text{OH}$  reaction. Accordingly, they suggested a value of  $2.0 \times 10^{13} \text{ cm}^3 \text{ mol}^{-1} \text{ s}^{-1}$  for the recombination/dissociation channel, yielding  $\text{HNO} + \text{H}$ . However, to the best of our knowledge, no experimental data are presently available. As expected, the recombination of  $\text{OH}$  and  $\text{NH}$  proceeds without any barrier, and the reaction  $\text{OH} + \text{NH} \rightarrow \text{HNOH}$  is exothermic by 67.1 kcal/mol. The initially formed energized  $\text{HNOH}$  has sufficient energy to either dissociate into  $\text{HNO} + \text{H}$  or isomerize into  $\text{NH}_2\text{O}$  followed by dissociation into  $\text{H} + \text{HNO}$  and  $\text{H}_2 + \text{NO}$ . The apparent rate constants of various channels for the  $\text{NH} + \text{OH}$  reaction are defined as:



The apparent rate constants for the formation of  $\text{NOH}_2$  **3** ( $k_3^C$ ) and  $\text{NOH} + \text{H}$  **7** ( $k_7^C$ ) were found to be very low and therefore will not be discussed any further. Figure 6 shows the variation of all apparent rate constants as a function of total pressure at 300 K. At this point, it should be noted that the magnitude of the apparent rate constants of all the channels as well as the total rate constant is highly dependent on the frequency factor ( $A(6)$ ) for the entry channel. We also found

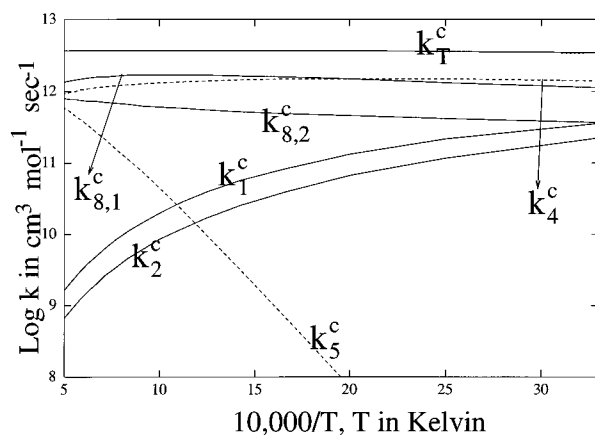


**Figure 7.** Plots of log apparent rate constants and total rate constant of  $\text{NH} + \text{OH}$  reaction versus  $10^4/T$  (K) at 1 atm.

that all the rate constants are almost proportional to  $A(6)$ . However, the variation of the rate constants as a function of temperature and pressure remains the same, and hence our calculations can predict correctly their behavior and product branching ratios. It is apparent that isomerization followed by dissociation into  $\text{H}_2 + \text{NO}$  ( $k_4^c$ ) is the predominant channel at low pressures. Also the apparent rate of formation of  $\text{HNO} + \text{H}$  from  $\text{NH}_2\text{O}$  ( $k_{8,1}^c$ ) is equally high and it contributes substantially to the total rate. It is interesting to note that  $k_{8,1}^c$  is consistently higher than  $k_{8,2}^c$ , which implies that the isomerization process is more favored over dissociation into  $\text{HNO} + \text{H}$ . This is again simply due to the lower barrier height for isomerization compared with dissociation from the  $\text{HNOH}$  potential well.  $k_2^c$  increases with increasing pressures and reaches a limiting value at high pressures while  $k_1^c$  decreases at high pressures. This is evident from the fact that **2** to **1** isomerization is appreciable at low pressures. At high pressures, stabilization of **2** dominates over isomerization. The total apparent rate constant for  $\text{HNO} + \text{H}$  formation ( $k_{8,1}^c + k_{8,2}^c$ ) is slightly more than the apparent rate constant for  $\text{H}_2 + \text{NO}$  formation ( $k_4^c$ ), and hence the competitive products are expected to be  $\text{HNO} + \text{H}$  and  $\text{H}_2 + \text{NO}$ .

Figure 7 shows the variation with temperature of the apparent rate constants at 1 atm. At all temperatures, dissociation into  $\text{HNO} + \text{H}$  and  $\text{H}_2 + \text{NO}$  are invariably more favored over stabilization of either adducts and the total rate constant remains almost constant over the entire temperature range. Our calculated total rate constant for the disappearance of  $\text{NH} + \text{OH}$  amounts to  $1.60 \times 10^{13} \text{ cm}^3 \text{ mol}^{-1} \text{ s}^{-1}$ .

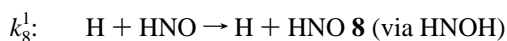
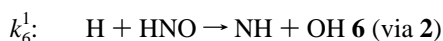
#### QRRK Analysis of the $\text{H} + \text{HNO}$ Reaction (Reaction D).

The  $\text{H} + \text{HNO}$  reaction can give rise to either  $\text{NH}_2\text{O}$  **1** or  $\text{HONH}$  **2** as the initially formed energized adduct, and hence the kinetics of this reaction has been analyzed by starting from both  $\text{NH}_2\text{O}$  (reaction D-1) and  $\text{HNOH}$  (reaction D-2) potential wells. We have also considered the direct hydrogen abstraction of  $\text{HNO}$  by  $\text{H}^\bullet$  giving rise to  $\text{H}_2 + \text{NO}$  in our kinetic analysis. The several product channels that are energetically possible include  $\text{NH}_2\text{O}$ ,  $\text{HNOH}$ ,  $\text{H}_2 + \text{NO}$ ,  $\text{NH} + \text{OH}$ , and  $\text{NH}_2 + \text{O}$  (Figure 1).

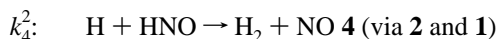
The various possible competitive reactions starting from  $\text{H} + \text{HNO}$  are shown in Scheme 1. Two distinct adducts can be formed depending on the addition of a hydrogen atom to either the nitrogen or the oxygen atom of  $\text{HNO}$  species. Since the rate constants for product formation depend heavily on the internal energy of the adduct, the product distributions originating from these two additions are expected to differ markedly.

The calculated barriers for H-addition to the nitrogen and the oxygen atom of  $\text{HNO}$  are 4.5 and 8.4 kcal/mol, respectively.

For the reaction D-1, we define the apparent rate constants for the various pathways in Scheme 1 as follows:



Similarly, for the reaction D-2:



Recall that the superscript and subscript in the rate constant definition correspond to the reaction and product numbers, respectively, as shown in Scheme 1. The apparent rate constants,  $k_3^1$ ,  $k_7^1$ ,  $k_3^2$ ,  $k_7^2$  are very low due to the high activation barrier for  $\text{NOH}_2$  **3** formation. These pathways therefore have little importance in the destruction of the reactants. The total rate constant for the disappearance of the reactants was calculated as the sum of all apparent rate constants, except for  $k_8^1$  and  $k_8^2$ , since these channels regenerate the reactants  $\text{H} + \text{HNO}$ . Figure 8 displays the variation of the apparent rate constants for reactions D-1 and D-2 as a function of total pressure at 300 K. The total rate constant for the disappearance of  $\text{H}$  and  $\text{HNO}$  remains almost constant over the pressure range of  $10^{-6}$ –0.01 atm and the main contribution to the total rate constant, in this pressure range, is the  $k_4^1$  channel leading to the concerted elimination products,  $\text{H}_2$  and  $\text{NO}$ . At high pressures ( $>0.1$  atm), stabilization of  $\text{H}_2\text{NO}$  **1** and  $\text{HNOH}$  **2** outruns their dissociation into  $\text{H}_2 + \text{NO}$ . In the lower pressure region, the

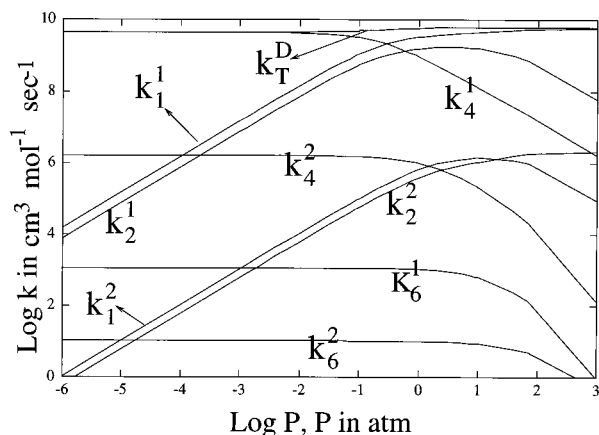


**Figure 8.** Plots of log apparent rate constants and total rate constant of H + HNO reaction versus log pressure at 300 K.

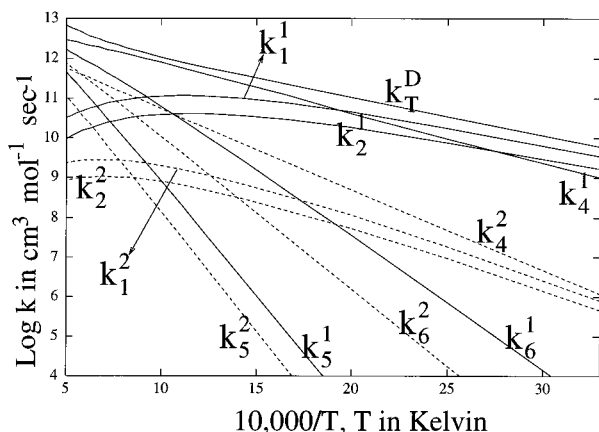


**Figure 9.** Plots of log apparent rate constants and total rate constant of H + HNO reaction versus  $10^4/T$  (K) at 1 atm.

rate of formation of adducts ( $k_1^1$ ,  $k_2^1$ ,  $k_3^2$ ,  $k_3^1$ ) increases with increasing pressures. However, in the high-pressure region, while  $k_1^1$  and  $k_2^2$  reach a limiting value,  $k_2^1$  and  $k_1^2$  decrease after passing through a maximum. This is likely due to the fact that at lower pressures  $1 \rightarrow 2$  or  $2 \rightarrow 1$  isomerization is appreciable even though the main channel is  $1 \rightarrow \text{H}_2 + \text{NO}$  ( $k_4^1$ ). At very high pressures, the initially formed adduct **1** (reaction D-1) or **2** (reaction D-2) gets stabilized at the cost of isomerization, thereby reducing the stabilization rate for the other isomer. Figure 9 displays the variation of all the apparent rate constants for reactions D-1 and D-2 with temperature at atmospheric pressure. At low temperatures, stabilization of  $\text{NH}_2\text{O}$  and  $\text{HNOH}$  seems to be predominant. The  $k_4^1$  channel opens up at high temperatures. In other words, at low pressures and at all temperatures,  $k_4^1$  is the predominant channel, while at high pressures,  $k_4^1$  becomes a main channel only at high temperatures. The total rate constant for reaction D-2 is more than 3 orders of magnitude lower than that for reaction D-1 due to the fact that the barrier for addition to the oxygen atom of HNO (8.4 kcal/mol) is somewhat higher than that to the nitrogen (4.5 kcal/mol). Nevertheless, HNOH formed in reaction D-1 plays no doubt an important role in the kinetics of H + HNO reaction.

The direct hydrogen abstraction (D-3) rate constant,  $k_{\text{DH}}^{\text{D}}$  was calculated by using the Arrhenius rate expression with 0.2 kcal/mol activation barrier. The frequency factor was calculated from the partition function of **4/8**, H and HNO. The value of  $k_{\text{DH}}^{\text{D}}$  and  $k^{\text{D}}$  ( $= k_{\text{DH}}^{\text{D}} + k_{\text{T}}^{\text{D}}$ ) obtained from our calculation at 2000 K are  $6.74 \times 10^{13}$  and  $7.39 \times 10^{13} \text{ cm}^3 \text{ mol}^{-1} \text{ s}^{-1}$ , respectively. The calculated rate constant for the disappearance of H + HNO

is roughly a factor of 15 greater than that reported previously by Halstead and Jenkins ( $4.82 \times 10^{12} \text{ cm}^3 \text{ mol}^{-1} \text{ s}^{-1}$ ). For the very same reason discussed previously, the mismatch could be due to the poor description of the low-frequency vibration in the rate determining transition structure, **4/8**. The contribution of addition/isomerization/dissociation route ( $k_{\text{T}}^{\text{D}}$ ) to the total rate constant  $k^{\text{D}}$  is about 10% at 2000 K and atmospheric pressure. We have fitted the calculated rate constant to the standard three-parameter expression for use in combustion or atmospheric modeling studies. The rate constants are well represented over the entire temperature range by:

$$k_{\text{T}}^{\text{D}}(T) = 8.23 \times 10^8 T^{1.28} \exp(-1570/T)$$

$$k_{\text{DH}}^{\text{D}}(T) = 2.83 \times 10^8 T^{1.60} \exp(452/T)$$

$$k^{\text{D}}(T) = 1.37 \times 10^8 T^{1.70} \exp(491/T)$$

## Conclusion

Both electronic structure and rate theory calculations have been used to probe the reactions occurring on the lowest doublet PES of the  $[\text{H}_2\text{NO}]$  system. Geometries for stationary points on the PES are determined with the CCSD(T)/6-311++G(d,p) level of theory. With these geometries, relative energies are determined with CCSD(T)/6-311++G(3df,3pd) calculations.

Direct hydrogen abstraction reaction is identified as the main channel of the  $\text{H}_2 + \text{NO}$  process, and it contributes predominantly to the total rate constant of the reaction. The addition intermediates on the doublet potential energy surface are  $\text{NH}_2\text{O}$  **1**,  $\text{HNOH}$  **2**, and  $\text{NOH}_2$  **3**. The competitive product channels are  $\text{H}_2 + \text{NO}$ ,  $\text{H} + \text{HNO}$ , and  $\text{NH} + \text{OH}$ . The thermodynamically stable product,  $\text{H}_2\text{NO}$ , can be stabilized only at high pressures in the reactions of  $\text{NH}_2$  with O. Our calculated total rate constant for  $\text{NH}_2 + \text{O}$  amounts to  $6.43 \times 10^{13} \text{ cm}^3 \text{ mol}^{-1} \text{ s}^{-1}$  and is in good agreement with the experimental value of Adamson et al.<sup>17</sup> Rate expressions are also derived on the basis of modified Arrhenius equation for the predominant pathways in all the reactions investigated here. Our calculated results show that for reaction C, the formations of  $\text{H}_2 + \text{NO}$  and  $\text{H} + \text{HNO}$  are equally competing channels and the most favorable product, for reaction D, from the intermediate as well as from the direct hydrogen abstraction is the  $\text{H}_2 + \text{NO}$ . The calculated total rate constant for reaction D is  $7.39 \times 10^{13} \text{ cm}^3 \text{ mol}^{-1} \text{ s}^{-1}$  and is a factor of 15 greater than the experimental values. The heats of formation of the stable isomers are calculated to be:  $\Delta H_f^0(\text{H}_2\text{NO}) = 18.3$ ,  $\Delta H_f^0(\text{HNOH}) = 24.8$  at 0 K,  $\Delta H_f^{298}(\text{H}_2\text{NO}) = 17.5$  and  $\Delta H_f^{298}(\text{HNOH}) = 23.7$  kcal/mol at 298 K with an uncertainty of  $\pm 2$  kcal/mol.

**Acknowledgment.** We are indebted to the Fund for Scientific Research (FWO-Vlaanderen) and Geconcerteerde Onderzoeksakties (GOA) for financial support and to the KU Leuven Computer center for providing computer facilities.

## References and Notes

- Keana, J. F. W. In *Spin-Labeling Theory and Applications*; Berliner, J. L., Ed.; Academic Press: New York, 1979; p 115–172.
- Bozzelli, J. W.; Dean, A. M. In *Combustion Chemistry*, 2nd ed; Gardiner, W. C., Ed.; 1995.
- Ando, H.; Asaba, R. *Int. J. Chem. Kinet.* **1976**, *8*, 259.
- Flower, W. L.; Hanson, R. K.; Kruger, C. H. *Combust. Sci. Technol.* **1977**, *15*, 115.
- Natarajan, K.; Mick, H. J.; Woiki, D.; Roth, P. *Combust. Flame* **1994**, *99*, 610 and references therein.
- Diau, E. W.; Halbgewachs, M. J.; Smith, A. R.; Lin, M. C. *Int. J. Chem. Kinet.* **1995**, *27*, 867.



- (7) Soto, M. R.; Page, M. J. *Chem. Phys.* **1992**, 97, 7287.  
(8) Walch, S. P. J. *Chem. Phys.* **1993**, 99, 3804.  
(9) Clyne, M. A. A.; Thrush, B. A. *Discuss. Faraday Soc.* **1962**, 33, 139.  
(10) Bulewicz, E. M.; Sudgen, T. M. *Proc. R. Soc. London* **1964**, 277, 143.  
(11) Lambert, R. M. *J. Chem. Soc., Chem. Commun.* **1966**, 850.  
(12) Kohout, F. C.; Lampe, F. W. J. *Chem. Phys.* **1967**, 46, 4075.  
(13) Halstead, C. J.; Jenkins, D. R. *Chem. Phys. Lett.* **1968**, 2, 281.  
(14) Smith, M. Y. *Combust. Flame* **1972**, 18, 293.  
(15) Baulch, D. L.; Drysdale, D. D.; Horne, D. G.; Lloyd, A. C. *Evaluation of Kinetic Data for High-Temperature Reactions*; Butterworth: London, 1973; Vol. 1 and 2.  
(16) Page, M.; Soto, M. R. *J. Chem. Phys.* **1993**, 99, 7709.  
(17) Adamson, J. D.; Farhat, S. K.; Morter, C. L.; Glass, G. P.; Curl, R. F.; Phillips, L. F. *J. Phys. Chem.* **1994**, 98, 5665.  
(18) Misra, D. P.; Sauders, D. G.; Dagdigian, P. J. *J. Chem. Phys.* **1991**, 95, 955.  
(19) Misra, D. P.; Dagdigian, P. J. *Chem. Phys. Lett.* **1991**, 185, 387.  
(20) Yang, D. C.; Koszykowski, M. L.; Durant, J. C. *J. Chem. Phys.* **1994**, 101, 1361.  
(21) Duan, S.; Page, M. J. *Chem. Phys.* **1995**, 102, 6121.  
(22) Baker, J.; Butcher, U.; Dyke, J. M.; Morris, A. J. *Chem. Soc., Faraday Trans.* **1990**, 86, 3843.  
(23) Soto, M. R.; Page, M.; McKee, M. L. *Chem. Phys. Lett.* **1991**, 187, 335.  
(24) Cai, Z. L. *Chem. Phys.* **1993**, 169, 75.  
(25) Barone, V.; Grand, A.; Minichino, C.; Subra, R. *J. Phys. Chem.* **1993**, 97, 6355.  
(26) Ricca, A.; Weber, J.; Hanus, M.; Ellinger, Y. *J. Chem. Phys.* **1995**, 103, 274.  
(27) Dean, A. M. *J. Phys. Chem.* **1985**, 89, 4600.  
(28) Bozzelli, J. W.; Dean, A. M. *J. Phys. Chem.* **1989**, 93, 1058; **1993**, 97, 4427.  
(29) Sengupta, D.; Chandra, A. K. *J. Chem. Phys.* **1994**, 101, 3906.  
(30) Nguyen, M. T.; Sengupta, D.; Vanquickenborne, L. G. *Chem. Phys. Lett.* **1995**, 240, 513.  
(31) Nguyen, M. T.; Sengupta, D.; Raspoet, G.; Vanquickenborne, L. G. *J. Phys. Chem.* **1995**, 99, 11883.  
(32) Nguyen, M. T.; Sengupta, D.; Vereecken, L.; Peeters, J.; Vanquickenborne, L. G. *J. Phys. Chem.* **1996**, 100, 1615.  
(33) Nguyen, M. T.; Sengupta, D.; Vanquickenborne, L. G. *J. Phys. Chem.* **1996**, 100, 10956.  
(34) Sengupta, D.; Nguyen, M. T. *Mol. Phys.* **1996**, 89, 1567; *Chem. Phys. Lett.* **1997**, 265, 35.  
(35) Frisch, M. J.; Trucks, G. W.; Gordon, M. H.; Gill, P. M. W.; Wong, M. W.; Foresman, J. B.; Johnson, B. G.; Schlegel, H. B.; Robb, M. A.; Replogle, E. S.; Gomperts, R.; Andres, J. L.; Raghavachari, K.; Binkley, J. S.; Gonzalez, C.; Martin, R. J.; Fox, D. J.; Defrees, B. J.; Baker, J.; Stewart, J. J. P. and Pople, J. A. *Gaussian 94*; Gaussian Inc.: Pittsburgh, PA, 1994.  
(36) Wolf, M.; Yang, D. L.; Durant, J. L. *J. Photochem. Photobiol., A* **1994**, 80, 85.  
(37) Lin, M. C.; Hsu, C.-C.; Kristyan, S.; Melius, C. F. *Proc. 1996 JANNAF CS-PSHS Joint Meeting*.  
(38) Dean, A. M.; Westmoreland, P. R. *Int. J. Chem. Kinet.* **1987**, 19, 207.  
(39) Weston, R. E. *Int. J. Chem. Kinet.* **1986**, 18, 1259.  
(40) Robinson, P. J.; Holbrook, K. A. *Unimolecular Reactions*; Wiley-Interscience: London, 1972.  
(41) Troe, J. *J. Chem. Phys.* **1977**, 66, 4758.  
(42) Troe, J. *J. Phys. Chem.* **1979**, 83, 114.  
(43) Hippler, H.; Troe, J.; Wendelken, J. *J. Chem. Phys.* **1983**, 78, 6709.  
(44) Melius, C. F.; Binkley, J. S. *20th Symp. (Int.) Combust., Proc.*; The Combustion Institute: Pittsburgh, 1984; pp 575–83.  
(45) Gehring, M.; Hoyeremann, K.; Schacke, H.; Wolfrum, J. In *14th Symposium (Int.) on Combustion*; The Combustion Institute: Pittsburgh, 1973; p 99.  
(46) Dransfeld, P.; Hack, W.; Kurzke, H.; Temps, F.; Wagner, H. Gg. In *20th Symposium (Int.) on Combustion*; The Combustion Institute: Pittsburgh, 1984; p 655.  
(47) Cohen, N.; Westburg, K. R. *J. Phys. Chem. Ref. Data* **1991**, 20, 1211.